

UC San Diego

UC San Diego Electronic Theses and Dissertations

Title

Engineering Gold-Silica Nanoparticle for Enhanced Photoacoustic Imaging

Permalink

<https://escholarship.org/uc/item/58p3x0dk>

Author

Lu, Tianyi

Publication Date

2019

Peer reviewed|Thesis/dissertation

UNIVERSITY OF CALIFORNIA SAN DIEGO

Engineering Gold-Silica Nanoparticle for Enhanced Photoacoustic Imaging

A Thesis submitted in partial satisfaction of the
requirements for the degree

Master of Science

in

Bioengineering

by

Tianyi Lu

Committee in Charge:

Professor Ratneshwar Lal, Chair
Professor Adam J. Engler
Professor Ester Kwon

2019

Copyright

Tianyi Lu, 2019

All rights reserved.

The Thesis of Tianyi Lu is approved, and it is acceptable in quality and form for publication on microfilm and electronically:

Chair

University of California San Diego

2019

Table of Contents

Signature Page	iii
Table of Contents	iv
List of Figures	v
List of Tables.....	vi
Acknowledgements.....	vii
Abstract of the Thesis	viii
1. Introduction.....	1
1.1. Photoacoustic Imaging.....	1
1.1.1. Principles of Photoacoustic Imaging	1
1.1.2. Contrast Agent of Photoacoustic Imaging	2
1.1.3. PAI Combined with Theranostics	3
1.2. Silica Nanobowl Template	4
1.2.1. Structure of Silica Nanobowl.....	4
1.2.2. Applications of Silica Nanobowl	5
2. Materials & Methods	7
2.1. Synthesis of Gold-Silica Nanoparticle.....	7
2.2. Characterizations.....	10
2.2.1. SEM	10
2.2.2. DLS & Zeta Potential.....	10
2.2.3. Absorbance Spectrum	10
2.2.4. Photoacoustic Imaging.....	11
3. Results & Discussion	12
3.1. Morphology Analysis.....	12
3.2. Spectrum of Gold Plasmon	17
3.3. Photoacoustic Imaging.....	19
4. Conclusion	23
References.....	24

List of Figures

Figure 1. Schematics for Silica Nanobowl and Gold Plasmon.....	5
Figure 2. SEM Images of Silica Nanobowl	12
Figure 3. TEM & SEM Image of Gold Nanoparticle Seeded on Nanobowl	13
Figure 4. SEM Images of Six Different Gold Nanoclusters & Photos of Aqueously Dispersed Gold Nanoclusters.....	14
Figure 5. DLS Profiles of Gold Nanoclusters.....	15
Figure 6. Zeta Potential Profiles of Gold Nanoclusters	16
Figure 7. SEM Images of Gold Nanoclusters Using Potassium and Sodium GS.	17
Figure 8. Absorbance Spectrum of Gold Plasmon.....	19
Figure 9. Photoacoustic Response: spectrum (left) and PA images (right).....	22

List of Tables

Table 1. Relative PA Response per Mole Gold at 700 nm..... 22

Acknowledgements

I would like to acknowledge Dr. Deependra Ban from Lal Lab for helping me with experiment design and material characterizations of SEM, TEM and PAI. I would also like to acknowledge Junxiang Zhao from Liu Lab for helping with darkfield scattering spectrum and Junxin Wang from Jokerst Lab for helping with PAI setups and experiments. I would like to acknowledge Nano3 staff for their assistance with SEM and Sailor Lab for providing DLS instrument. Finally, I would like to thank my parents and my most sincere friends of the past ten years for supporting me psychologically through tough moments of this period.

Abstract of the Thesis

Engineering Gold-Silica Nanoparticle for Enhanced Photoacoustic Imaging

by

Tianyi Lu

Master of Science in Bioengineering

University of California San Diego, 2019

Professor Ratneshwar Lal, Chair

Plasmonic properties of gold nanoparticles have been studied intensively in recent years for various applications including catalysis and imaging. [1,2] In the field of Photoacoustic Imaging (PAI), plasmonic gold is particularly interesting since localized resonance of gold plasmon could cause a red-shift in its absorption spectrum that is possible to fit the near-infrared range of commonly used excitation laser in PAI. [3] In this thesis, we report on using a controllable

bottom-up method to develop clustered plasmonic gold nanoparticles localized on silica nanoparticle, that serves as an effective contrast agent in PAI. The results of photoacoustic imaging and spectroscopy show a significant higher contrast in these plasmonic gold nanoparticles compared to non-clustered gold nanoparticles.

1. Introduction

1.1. Photoacoustic Imaging

1.1.1. Principles of Photoacoustic Imaging

Photoacoustic (PA) effect was first discovered by Alexander Bell and his colleagues in the late 19th century. [4] The essence of this phenomenon is that molecules absorb energy from incident light and converts into collisional energy, which causes thermoelastic expansion and thus emission of sound waves. [5] Based on this phenomenon, laser can be used to generate ultrasound in locations of interest. Compared to traditional ultrasound imaging techniques, this new technique has much higher resolution due to the high selectivity and accuracy of laser, while preserving the high penetration of ultrasound.

To generate sound waves effectively in PAI, pulsed laser excitation is commonly used. [6] Pulsed laser has the advantage of high signal-to-noise ratio compared to continuous-wave. The duration of pulsed laser excitation should be much less than stress confinement time and thermal confinement time so that during excitation, volume expansion and thermal diffusion can be neglected. Consequently, the absorbed laser energy transits into pressure gradient near the illuminated molecule. The pressure change can be expressed as

$$P=\beta A/\rho C_v \kappa,$$

where β is thermal coefficient of volume expansion, A is intensity of absorption, ρ is the density of the material, C_v is specific heat capacity at constant volume and κ is isothermal compressibility. [7]

In the past few decades, benefitting from rapid development of computational technology, image reconstruction based on PA signal has also made progress, which makes it possible to acquire high-quality images using PA effects. Using spherical detector aperture and rectilinear-scanning detector arrays, Kruger et al were able to image human breasts by PAI at depth of 53 mm and with 0.42mm spatial resolution, which is much higher than traditional ultrasound imaging under similar depth of field. [8] Highly tissue-specific light absorption allows researchers to acquire images of lipids and hemoglobin that show significant contrast compared to neighboring soft tissues, which is not very likely in pure ultrasound imaging. [9] Doppler effect, which is a common modality in traditional ultrasound imaging, can also be utilized in PAI to study subtle circulation phenomena such as they blood flow study of microvasculature in mouse ear and chicken embryo by Yao et al. [10] As more modalities are added and computational methods are improved for higher resolution and contrast, PAI would become a more comprehensive and powerful tool in biomedical imaging.

1.1.2. Contrast Agent of Photoacoustic Imaging

A critical limitation of PAI is that exogenous contrast agent is often required in this modality since biological tissues do not possess good PA response. [11] Organic dyes such as Indocyanine-green (ICG) and Methylene-blue (MB) are commonly used. However, due to their vulnerable photolytic stability, the effectiveness of these organic molecules decreases significantly during long-time imaging process. This drawback is especially concerning in Photoacoustic Tomography, which could take more than ten minutes in large animals.

To overcome this problem, plasmonic noble metal nanoparticles of different sizes and structures are studied for their PA response. Commonly noble metals such as gold and silver have much higher absorption than organic dyes, which consequently leads to higher intensity of PA response in noble metals. [11] In addition, localized surface plasmon resonance (LSPR) allows modification in terms of size and morphology that further mediates the optical absorption of noble metal to serve as contrast agent in PAI. [12] Due to the low transmission of visible light in biological tissues, modified nanoparticles that possess high absorption in the near-infrared (NIR) range are more applicable for PAI than in the visible range. Gold nanoshells [13], gold nanorods [14] and embedded gold nanospheres [15] are common plasmon structures whose absorption peak can be tuned into NIR range.

1.1.3. PAI Combined with Theranostics

One imaging modality is often not adequate for comprehensive understanding of biological and physiological conditions and most researchers hope to combine different probing techniques together. Similarly, PAI can be fitted with other modalities of imaging and therapeutics. Cheng et al developed PEGylated WS₂ nanosheets that are functional in CT, PAI and photothermal therapy. [16] Ge et al developed carbon dots that are compatible with fluorescence, PAI and tumor diagnosis. [17] The mesoporous copper sulfide nanoparticles developed by Feng et al are capable of receptor-specific targeting, light-induced chemo-phototherapy and PA tomography, which is a good example in theranostics that combines diagnosis and therapy. [18] These nanomaterials all

possess high PA responses and their functionality in diagnosis or therapeutics greatly expands their applications in medicine. In this thesis, we aim to develop a nanomaterial based on an existing drug delivery system and this material is modified to provide high contrast in PAI.

1.2. Silica Nanobowl Template

1.2.1. Structure of Silica Nanobowl

Theranostic nanomedicine has been developing rapidly and provides researchers with plenty of different templates to perform drug delivery, imaging and therapeutics. [19] Due its biocompatibility, relative ease of fabrication and physical stability, systems of silica nanoparticles are widely explored in theranostics. [20] Therefore, we choose the drug delivery system of silica nanoparticles as our platform based on which a contrast agent for PAI is developed.

One silica nanoparticle, referred to as Nanobowl, is a versatile platform for catalysis and controlled theranostic delivery. [21] Nanobowl consists of one 100nm polystyrene core that is removable for specific purposes and one silica half shell that is chemically grown around the polystyrene core. The reason that this structure is called Nanobowl is that silica growth is controlled so that the polystyrene core is not fully covered, making it possible to create one cavity at the site of polystyrene core after polystyrene is dissolved or incinerated. The first two steps in Figure 1 demonstrate the synthesis of silica Nanobowl from polystyrene core.

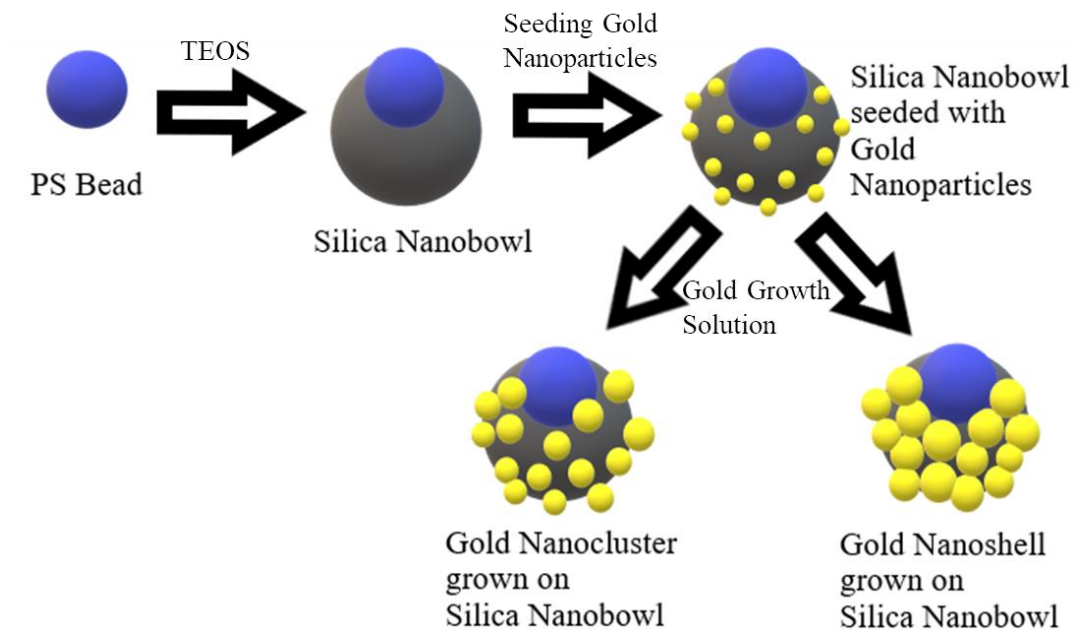


Figure 1. Schematics for Silica Nanobowl and Gold Plasmon

1.2.2. Applications of Silica Nanobowl

The rapidly developing technology in surface chemistry and bio-conjugation has enabled researchers to modify Nanobowl for various applications. According to the works of Mo et al, gold and magnetic iron oxide nanoparticles can be attached to the surface of Nanobowl, producing magnetically-responsive particles that enhance Surface-Enhanced Raman Spectroscopy (SERS). [22] A gold shell is grown on silica surface of Nanobowl and plasmon resonance of the gold shell provides distinct spectrum in NIR range. [22] However, the physical stability of this surface is impaired by the relatively weak electro-static interaction between gold and silica. In our project, we improve the method reported by Mo et al, by embedding small gold nanoparticles (3~5nm in diameter) on the surface of silica carrier using covalent conjugation and subsequently growing gold in a controlled manner to optimize the gold surface for PAI. Compared to gold

nanoparticles synthesized via sodium citrate method [22], THPC method [23] provides smaller gold nanoparticles and gold growth is more controllable for these nanoparticles. As the last three steps in Figure 1 demonstrate, the 3~5nm gold nanoparticles serve as seeds and reduced free gold atoms are deposited on these seeds, leading to gold growth on the surface of silica Nanobowl. Depending on the size of seeding gold nanoparticles and the amount of gold growth solution, the morphology of gold plasma can become either clusters of gold nanoparticles (lower left step in Figure 1) or a gold shell as neighboring gold nanoparticles are all interconnected (lower right step in Figure 1).

2. Materials & Methods

2.1. Synthesis of Gold-Silica Nanoparticle

Nanobowl Preparation

Clean a magnetic stir bar in a 20mL glass vial (Fisher Scientific) with fresh aqua Regia, DI water, soap, DI water and IPA. Dry the vial in vacuum oven under 60 °C. Add 1.4mL H₂O, 2.6mL 30% ammonia (Fisher Scientific) and 8mL MP – methanol (Fisher Scientific) and 1-propanol (Acros Organics) mixture with ratio 3:2 – to a cleaned vial and place the vial on magnetic mixer. Take 0.5mL 100nm carboxyl-polystyrene bead (PS-COOH)(Polysciences) and perform vortex mixing for 10s. Simultaneously add 200µL PS-COOH and 110µL tetraethyl orthosilicate (TEOS)(Sigma-Aldrich) to the glass vial while stirring, in 10s. Let the reaction proceed for 1h with stirring at room temperature. Collect the solution from the vial into a 15mL centrifuge tube. Centrifuge at 500RCF for 5min and collect supernatant. Centrifuge and wash the supernatant 3 times – centrifuge supernatant from 500RCF centrifugation at 3200RCF for 6min; discard new supernatant, add 3mL MP and disperse pellet with sonication for roughly 1min; repeat the whole process twice more. After purifying the sample for 3 times, disperse the pellet in 2mL MP and store the colloid at 4 °C.

Nanobowl Surface Modification

Prepare a cleaned tube with one magnetic stir bar. Disperse the sample from previous step with sonication for 10s to reverse possible reversible aggregation during storage. Transfer the 2mL sample to the tube and dilute it with 2mL MP. Place the tube in silicon oil bath at 60 °C with continuous magnetic

stirring. After 5min, add 10.6 μ L 3-aminopropyltriethoxysilane (APTES)(Fisher Scientific) to the reaction vessel in 3s. Let the reaction proceed for 2h at 60 °C. After completion of reaction, collect the mixture and purify the product with 3 times of centrifugation and wash – same as the purification method utilized in the previous step.

Complete buffer change from MP to PBS 1x (Thermo Fisher Scientific) by 3 times of centrifugation and redispersion. Disperse all purified Nanobowl in 6mL PBS. Prepare 1mL of EDC/PBS solution with 15mg EDC powder (Thermo Fisher Scientific). Prepare 1mL of NHS/PBS solution with 27mg NHS powder (Sigma-Aldrich). Prepare 6mL 3MPA/PBS solution with 13.8 μ L 3MPA. Prepare 3 cleaned glass vials each with one magnetic stir bar. In each vial, mix 2mL 3MPA/PBS solution and 40 μ L EDC/PBS solution; put glass vials on stirring; after 2min, add 42 μ L NHS/PBS solution to each vial; after 1min, add 2mL Nanobowl/PBS solution to each vial in 15s. Let the reaction proceed for 2h at room temperature. Collect all the solutions from 3 vials into one 15mL centrifuge tube and perform purification – centrifuge the initial solution at 3200RCF for 10min; discard supernatant, wash pellet with 2mL H₂O and disperse it with sonication for 2-4min; repeat the process except centrifuging the colloid at 3200RCF for 5min. Disperse final pellet in 4mL PBS with sonication.

Gold Nanoparticle Preparation

Prepare a fresh stock solution of 10M NaOH(aq) using NaOH pellets (Sigma-Aldrich). In a 50mL centrifuge tube, mix 30.58mL DI H₂O, 27.3 μ L 10M NaOH(aq) and 6.5 μ L Tetrakis(hydroxymethyl)phosphonium chloride

(THPC)(Sigma-Aldrich). Put the mixture on slow vortex for 5min. Add 237 μ L 100mM HAuCl₄(aq) to the reaction vessel slowly. Let the reaction proceed for 1h at room temperature while stirring. Then store the solution at 4 °C. HAuCl₄(aq) is prepared by dissolving gold chloride trihydrate (Sigma-Aldrich) in DI H₂O at room temperature.

Gold Seeding on Nanobowl

Disperse the 4mL Nanobowl/PBS acquired from surface modification with 20s sonication. Prepare 4 cleaned glass vials with magnetic stir bars. Add 1mL Nanobowl/PBS and 2mL H₂O to each vial. Put all vials on magnetic stirring plate. To each vial, add 2.25mL gold nanoparticle solution in 10s. Let the mixtures be stirred for 30min and then incubate at 4 °C overnight. Centrifuge and wash the reactants 4 times with H₂O – set centrifugation at 3200RCF for 5min for each step; wash the initial pellet with 2mL H₂O per tube; mix all dispersed Nanobowls into one centrifuge tube and proceed with standard purification process. Final pellet is dispersed in 6mL H₂O.

Gold Nanoparticle Growth

In a cleaned glass vial with stir bar, mix 0.25mL seeded Nanobowl solution with 4mL H₂O and put the solution on magnetic stirring plate. Prepare gold growth solution (GS) of 13mM HAuCl₄ and 53.7mM K₂CO₃ (Fisher Scientific). Prepare reducing solution (RS) of 11mM NH₂OH·HCl (S A Chemical Products). While stirring the Nanobowl solution, simultaneously add GS and RS to the glass vial at 0.025mL/min using syringe pump. Let the reaction proceed for 20min. After reaction is complete, transfer all solution to a centrifuge tube and

perform purification procedure four times as described in previous sections – centrifugation is set at 3200RCF for 5min; wash pellet with 2mL H₂O; disperse final pellet in 2mL H₂O.

2.2. Characterizations

2.2.1. SEM

Morphology characterization of anobowl and its surface-modified products is performed via Scanning Electron Microscopy (SEM) (Zeiss Sigma 500). Samples are prepared by depositing 5 μ L aliquots on aluminum SEM post. In imaging, 3-5kV voltage is commonly applied to the post. The images are analyzed for size of Nanobowl, number of pores, number of gold nanoparticles per Nanobowl, size of gold nanoparticles, percentage of aggregated Nanobowl.

2.2.2. DLS & Zeta Potential

Dynamic Light Scattering (DLS) apparatus (Malvern Instruments Zetasizer Nano) is used to determinate size distribution of Nanobowls in aqueous solution. On the same instrument, multi-purpose titrator for zeta potential is used to determine zeta potential of the samples. These measurements aim to characterize stability of the nanoparticles in aqueous environment.

2.2.3. Absorbance Spectrum

Absorbance spectrum of all samples is acquired via absorbance scan in a UV-VIS plate reader (Tecan Infinite 200 PRO). 100 μ L of each sample is transferred to one well in a 96-well transparent round-bottom plate (Corning) and scanned using absorbance scan mode. All sample are purified and dispersed in DI H₂O. A control of DI H₂O only is present for all measurements. Absorbance

spectrum is calculated by subtracting absorption of DI H₂O from absorption of dispersed samples. All spectra are normalized to analyze position and distribution of peaks in the spectra.

2.2.4. Photoacoustic Imaging

PAI is performed on a Vevo 2100 commercial photoacoustic scanner (Visualsonics). This system [24] consists of one flashlamp-pumped laser that operates around 20 Hz and scans between 680 and 970nm wavelength. This laser is coupled with 21 to 30 MHz ultrasound transducers (LZ250 and LZ400). All aqueous samples are filled in polyethylene tubing that is submerged in water. Six to seven tubing are measured simultaneously in each trial. The ultrasound transducers are placed about 1 cm above the tubing. Signal amplification is adjusted by changing gain parameters before each measurement, to achieve good signal-to-noise ratio and avoid over-exposure. A common range of gain is 10-40 dB for this project. Spectrum is acquired in 680-970nm range with step size of 1nm.

3. Results & Discussion

3.1. Morphology Analysis

The number of pores per Nanobowl is improved by changing solvents and reaction time. In Mo's paper, only ~30% silica Nanobowls contain one single pore and the rest contain more than one single pore. [21] By changing solvent from isopropanol (IPA) into a mixture of methanol and 1-propanol with 3:2 ratio and adjusting reaction time to 1 hour, we obtain silica Nanobowls in which ~50% (n=80) contain only one single pore, counted in Figure 2.A. This improvement in pore number would greatly enhance the physical and chemical stability of Nanobowls' surface. The diameter of silica Nanobowl is 296 ± 13 nm (n=8), counted in Figure 2.B.

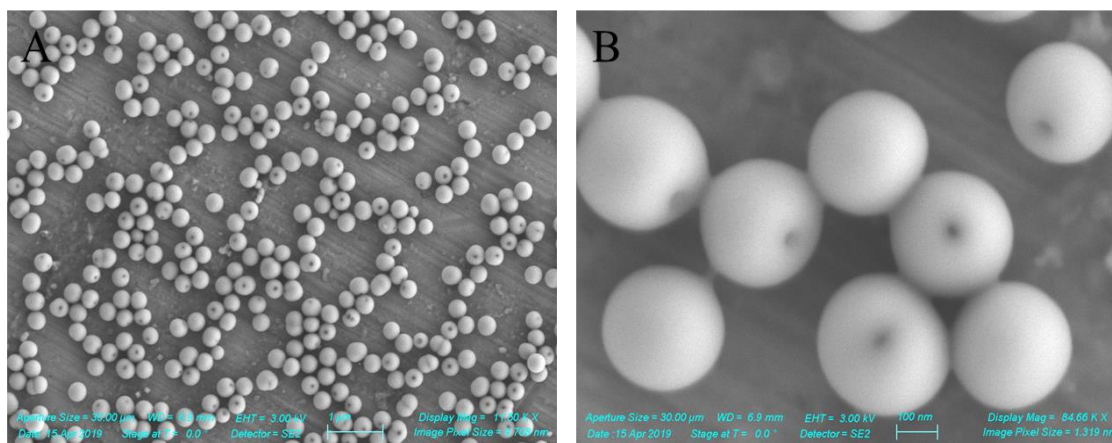


Figure 2. SEM Images of Silica Nanobowl

The gold nanoparticles synthesized by THPC method are characterized by TEM images after conjugation to silica Nanobowls. Since the actual resolution of SEM is limited, to characterize size and morphology of small gold nanoparticles, TEM is used. As shown in Figure 3, gold nanoparticles are visible in the TEM image of 3.A but only larger gold nanoparticles at certain angles to incident

electron beam are visible with blurry boundaries in the SEM image of 3.B. The diameter of embedded gold nanoparticles is measured from Figure 3.A as 5.0 ± 1.2 nm ($n=18$). The advantage of using these smaller gold seeds, compared to gold nanoparticles with a typical diameter around 15 nm, is that growth of gold is more controllable. In Mo's paper, gold growth occurs relatively fast and a full shell is produced in this process. Using smaller gold seeds, we are able to control the size of gold nanoparticles so that they form multiple clusters on the silica surface instead of a full gold shell wrapping the silica surface.

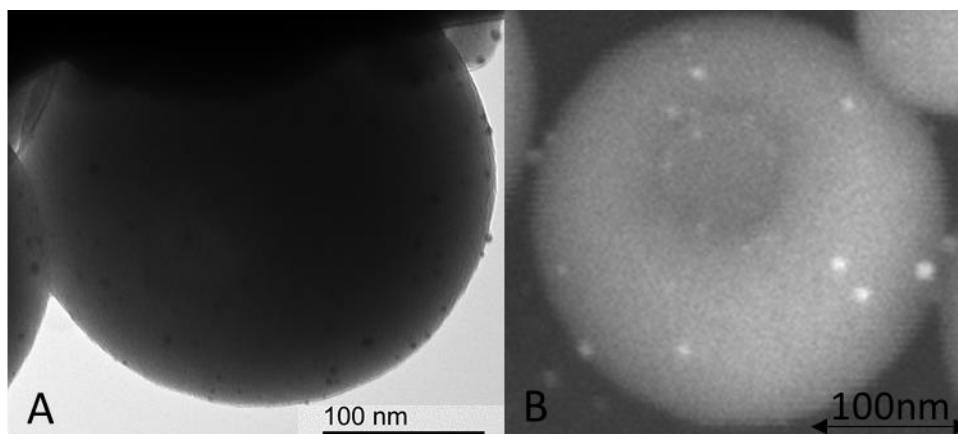


Figure 3. TEM & SEM Image of Gold Nanoparticle Seeded on Nanobowl

After storing gold nanoparticles synthesized by THPC method at 4 °C for one week, we obtain gold seeds that are much larger in size, which we refer to as aged seeds while newly synthesized gold nanoparticles by THPC method that are ~5nm in diameter are referred to as new seeds. Using these two different seeds for embedment, we observe difference in their structures after gold growth process. In Figure 4, six different kinds of gold clusters are investigated. The gold seeds used in A, B and C are new seeds and those used in D, E and F are aged seeds. Gold growth solution (GS) is added into aqueously dispersed seeded Nanobowls with a

molar ratio of 6:1 for B and E. 80% GS is used for A and E; 120% GS is used for C and F. The structures illustrated in Figure 4 show that gold cluster tends to be more like a shell for larger seeds and higher amount of GS.

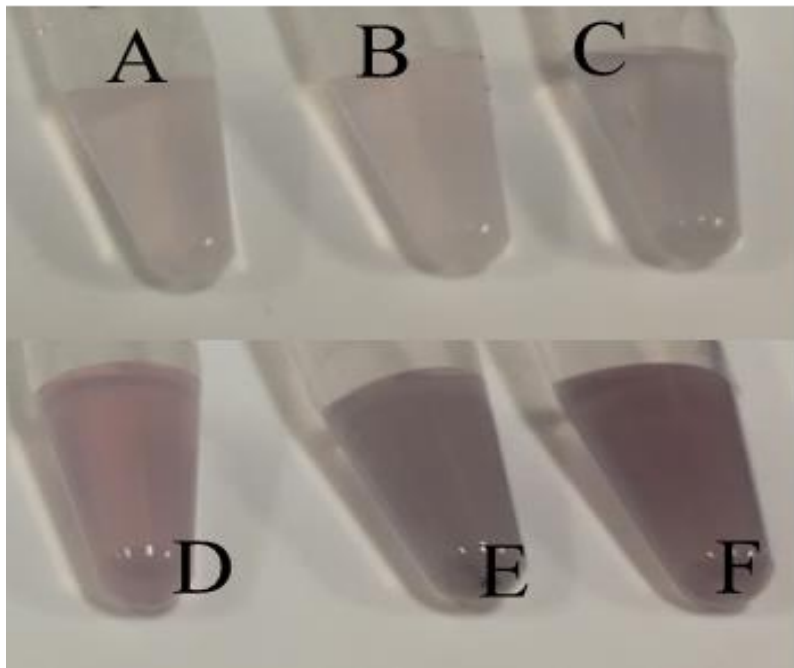
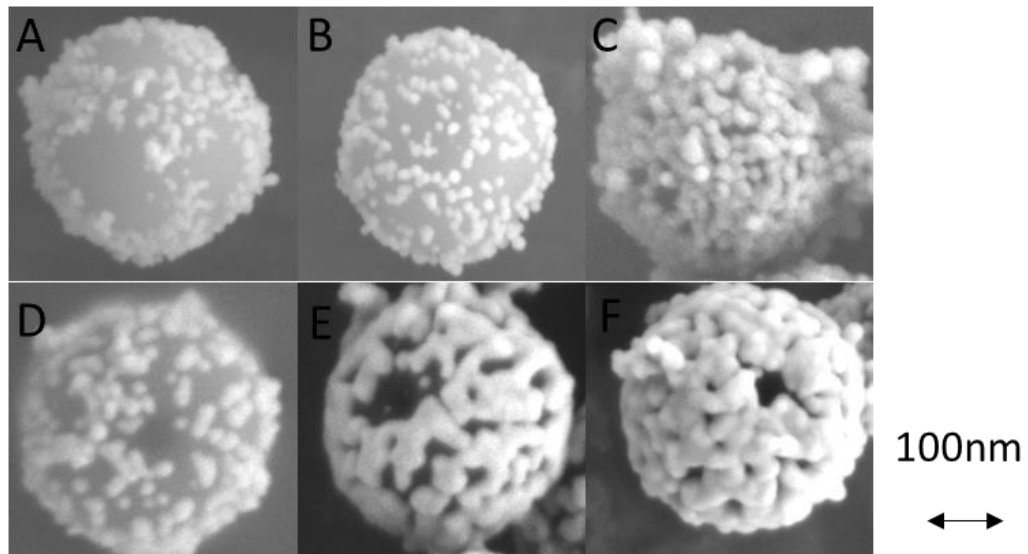


Figure 4. SEM Images of Six Different Gold Nanoclusters & Photos of Aqueously Dispersed Gold Nanoclusters

To verify how these nanoparticles exist in aqueous environment, specifically their hydrodynamic size and zeta potential, we measure Dynamic Light Scattering (DLS) and zeta potential profiles. As the DLS profiles in Figure 5 shows, the hydrodynamic size of Nanobowls after gold growth is highly centered near 400 nm for all six kinds. The evidence for this statement is that, the number distribution, which demonstrates the population distribution of nanoparticles, is a sharp peak in all six samples. For intensity distribution profiles, a small peak near 5000 nm is present for sample B to E. Considering the relatively small proportion of these peaks (<2.5%) and the sharp single peak in each number distribution profile, we can conclude that even though a very small portion of aggregates may exist in our samples, the quantity of aggregation is quite low. Since the majority has hydrodynamic size around 400nm, which matches the size measurement from SEM image analysis, these gold nanoclusters can be considered as highly pure samples. Thus, the impact of particle aggregation on absorption spectrum and photoacoustic response can be neglected.

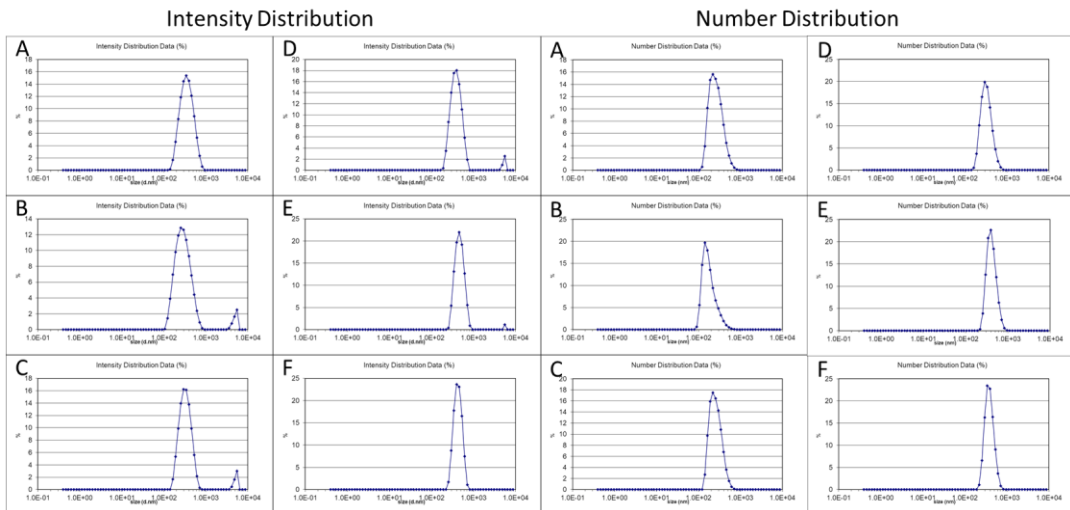


Figure 5. DLS Profiles of Gold Nanoclusters

The zeta potential profiles of sample B and E are investigated in Figure 6. The measured zeta potentials are relatively low, indicating that the nanoparticles in aqueous environment are not highly stable over time. The relatively unstable colloidal properties revealed by the zeta potential profiles explain the presence of very small amount of aggregation in DLS characterization. For this reason, in order to minimize effects of silica Nanobowl aggregation on optical and photoacoustic properties of gold nanoclusters on Nanobowl surface, SEM images are investigated for all samples analyzed for light spectroscopy and photoacoustic imaging.

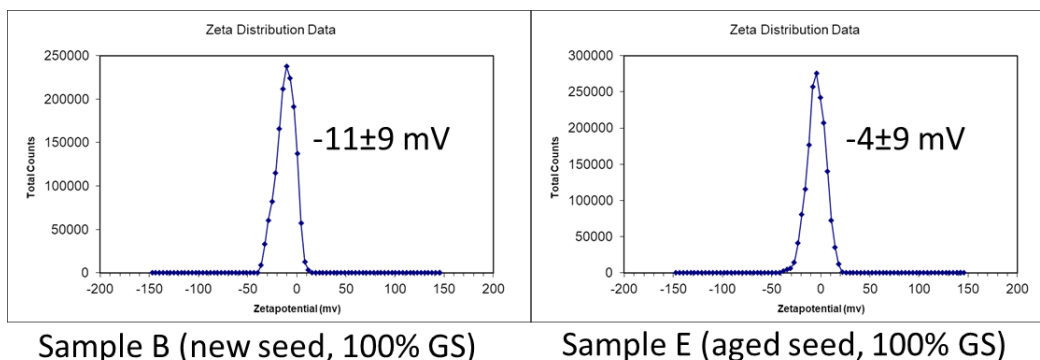


Figure 6. Zeta Potential Profiles of Gold Nanoclusters

Another method of using different cations to control gold growth and tune the gold nanoclusters for PAI is investigated. A set of experiments comparing sodium ion in GS with potassium ion is done. All conditions are maintained the same as conditions for sample B except for cations in GS. The SEM images comparing the gold nanoclusters formed in potassium GS and sodium GS are shown in Figure 7. The diameter of gold nanoclusters in Figure 7.A is measured to be 17.5 ± 1.8 nm ($n=20$) and the diameter of gold nanoclusters in Figure 7.B is measured to be 17.2 ± 2.7 nm ($n=20$). The p-value calculated for these two data

sets is 0.68 and thus, the null hypothesis is not rejected. Since no significant distinction is observed in terms of morphology of the nanoparticles, the endeavor to modify LSPR of gold nanoclusters by varying cations in GS fails.

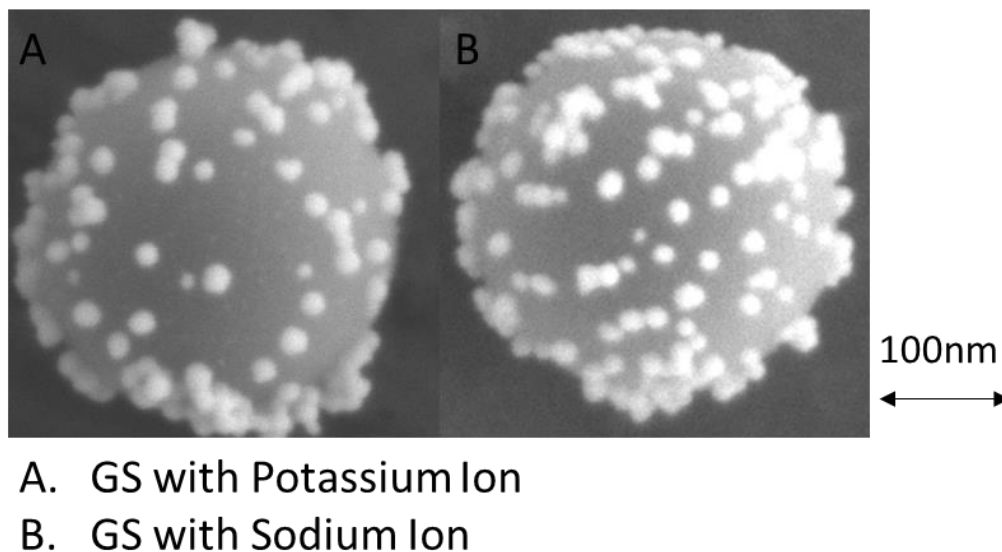


Figure 7. SEM Images of Gold Nanoclusters Using Potassium and Sodium GS

3.2. Spectrum of Gold Plasmon

Optical absorption is an important factor in PAI since acoustic energy is converted from absorbed photon energy. A comparison of six different gold nanoclusters along with silica Nanobowls embedded with the gold seeds before gold growth is shown in the normalized absorbance spectra in Figure 8. The goal of this analysis is to find the peaks in the spectra. The range 500-970 nm is selected for the spectra in Figure 8. The absorbance spectra for the two gold seeds are measured as a control group. The two gold seeds both have a peak around 520nm; this characteristic peak is shifted to ~550nm for gold nanoclusters after gold growth. This observation proves enhanced localized surface plasmon resonance (LSPR) in all six gold nanoclusters. In addition, a second peak appears

in the spectra of sample C, E and F: ~660 nm for C, ~700 nm for E and 670 nm for F. The appearance of a second peak is another evidence for plasmon resonance in the nanoclusters. This range of enhanced photon absorption matches the common 680-970 nm range of PAI.

However, it should be noted that the spectra do not show any information regarding absorption per unit mass. The most important information the spectra reveals is shift in peaks and supports our hypothesis that gold growth of seeding gold nanoparticles embedded on silica Nanobowl enhances photon absorption. To further verify if the gold nanoclusters are effective in PAI, spectrum of PA response is investigated in the next section.

Another problem that should be noted is that the measured spectra are noisier in the range between 850 nm to 970 nm. This phenomenon is caused by the limited operation range of our UV-VIS spectroscopy. Due to diffraction and much higher absorption of water and plates in infrared range, the measurement in this range via this instrument is less reliable. These effects are much less significant near 700 nm range and the conclusion of red-shift and enhanced absorption in near infrared range can be considered valid.

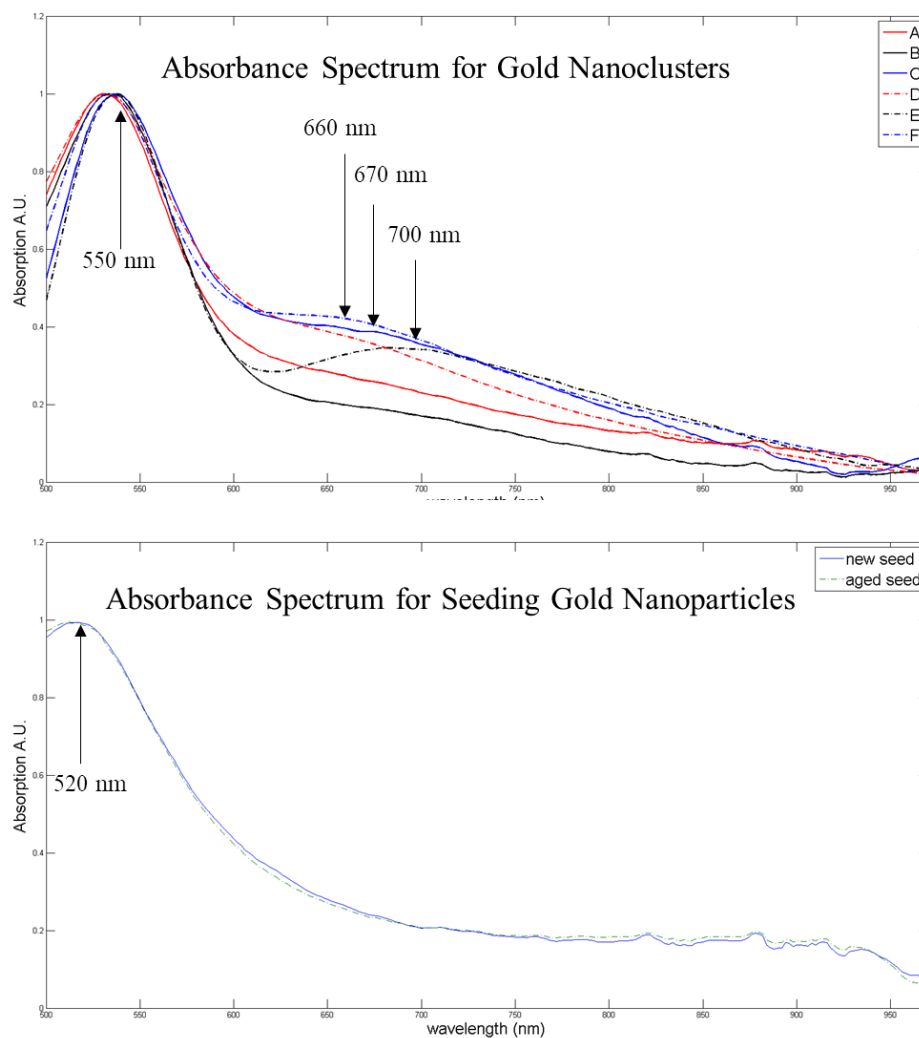


Figure 8. Absorbance Spectrum of Gold Plasmon

3.3. Photoacoustic Imaging

The six different kinds of gold nanoclusters are tested for their PA response. The left part of Figure 9 shows the spectrum of all six samples and the two different gold nanoparticles seeded on Nanobowl before gold growth. A distinct broad peak of 720-760 nm appears in the spectra of gold nanoclusters after gold growth, and seeded Nanobowls before gold growth show very weak PA response, compared to the other 5 samples. As Li et al points out, purely spherical

gold nanoparticles less than 100 nm do not have high absorption in NIR range and therefore could not contribute to a high PA response in this range. [25] This conclusion can explain the low PA response of seeding gold nanoparticles conjugated to silica Nanobowls since the gold nanoparticles are individual particles that are not clustered together. As the presence of gold nanoparticles does not contribute to the significantly enhanced PA response of A, B, C, E and F, this improvement can only be explained by LSPR of gold nanoclusters. It has been shown that similarly structured gold nanoshells and gold nanoclusters could be active PA contrast agent due to their high absorption property in NIR range. [26, 27] However, absorption is not the only factoring affecting PA response. The absorbance spectrum of sample D shows a similar absorption in 720-760 nm range compared to the other samples but its PA response in this range is significantly lower than the others. Comparing the PA response of sample A, B and C, we find that the highest PA response occurs in sample B; similarly the highest PA response among sample D, E and F occurs in sample E. Therefore, the amount of gold growth with molar ratio 6:1 relative to seeded Nanobowl is optimal for PA enhancement. The clustered gold nanoparticles of B and the shell-like gold nanoparticles of E have better PA response than the other gold nanoclusters. Compared to pure gold nanospheres that are around 20 nm in diameter which do not show distinctive peak in PA spectrum at NIR range, [28] the gold nanoclusters B and E possess one distinctive broad peak (720-760 nm) in NIR range on their PA spectra, indicating that these materials are better contrast agents for PAI than regular gold nanospheres.

The right part of Figure 9 shows a PA imaging of these samples loaded in tubing with probing laser at 700 nm. The black-and-white color bar is regular ultrasound imaging at B mode and the depth of the samples is 1cm below the ultrasound transducer. The cylindrical shapes of the tubing are shown in these images. The red color bar is imaging constructed from photoacoustic response. These PA images more directly show how PA responses are visualized. The redder the pixels are, the higher PA response the luminated area has. The seeded Nanobowls have barely no PA responses while the nanoclusters except sample D show distinctive red color in PAI. To quantitatively compare the PA responses, we calculate the PA response per mole gold for the eight samples, relative to new seed, in Table 1. PA response per quantity of material is a common parameter used to represent efficiency of contrast agent. From this table we find that PA efficiency of gold nanoclusters is over 10 times to that of seeding gold nanoparticles, proving that gold growth method is effective in producing gold colloidal that can be used in PAI. The samples with highest PA efficiency are B and E. Because PA response of free ICG (common organic dye) is about 4 orders of magnitude less than that of gold nanospheres less than 50 nm, [29] and the PA responses of sample B and sample E are 50 times stronger than that of small gold nanospheres, we can infer that PA efficiency of gold nanoclusters B and E would be significantly higher than the PA efficiency of free ICG. Combining with the conclusion from PA spectrum analysis, we can reach the conclusion that clustered gold nanoparticles in sample B and shell-like gold nanoparticles in sample E are optimized for the modality of photoacoustic imaging.

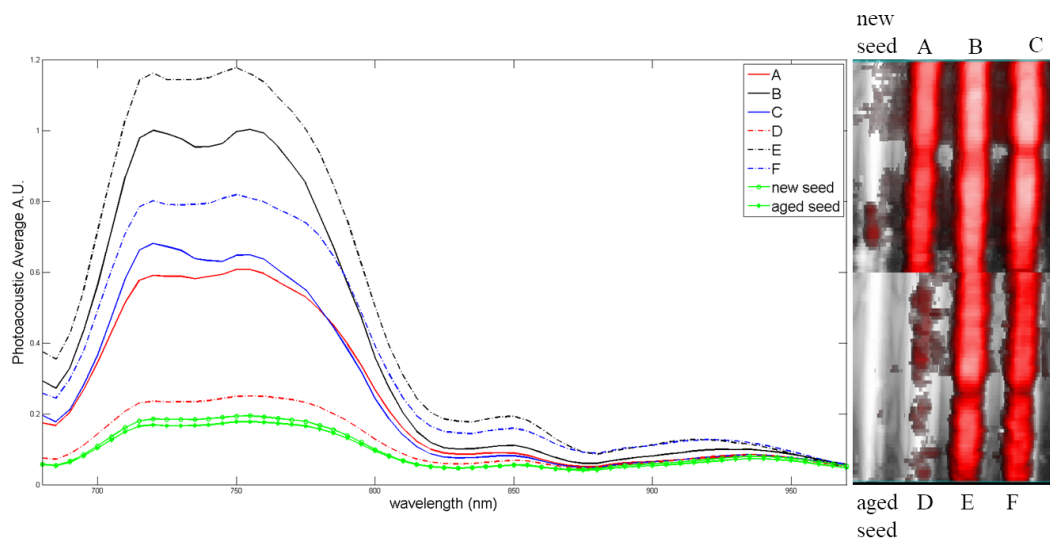


Figure 9. Photoacoustic Response: spectrum (left) and PA images (right)

Table 1. Relative PA Response per Mole Gold at 700 nm

Sample	new seed	aged seed	A	B	C	D	E	F
PA Average per mole gold	1.0	0.9	35.1	52.3	31.3	14.2	65.0	43.1

4. Conclusion

The two gold nanoparticles that are optimized for their PA responses (clustered gold nanoparticles and shell-like gold nanoparticles) show great performance in the operational NIR range of photoacoustic imaging, compared to common spherical gold nanoparticles. These properties make the materials a good candidate for contrast agent in PAI. In addition, the drug delivery capacity of the Nanobowl system on which the gold nanoclusters are built makes it a promising system that combines imaging, diagnosis and therapy.

References

1. Jia, Zixian, Mounir Ben Amar, Dezheng Yang, Ovidiu Brinza, Andrei Kanaev, Xavier Duten, and Arlette Vega-González. "Plasma catalysis application of gold nanoparticles for acetaldehyde decomposition." *Chemical Engineering Journal* 347 (2018): 913-922.
2. Dorsey, Jay F., Lova Sun, Daniel Y. Joh, Alon Witztum, Gary D. Kao, Michelle Alonso-Basanta, Stephen Avery, Stephen M. Hahn, Ajlan Al Zaki, and Andrew Tsourkas. "Gold nanoparticles in radiation research: potential applications for imaging and radiosensitization." *Translational cancer research* 2, no. 4 (2013): 280.
3. Link, Stephan, and Mostafa A. El-Sayed. "Spectral properties and relaxation dynamics of surface plasmon electronic oscillations in gold and silver nanodots and nanorods." (1999): 8410-8426.
4. Bell, Alexander Graham. "ART. XXXIV.--On the Production and Reproduction of Sound by Light." *American Journal of Science* (1880-1910) 20, no. 118 (1880): 305.
5. Xia, Jun, Junjie Yao, and Lihong V. Wang. "Photoacoustic tomography: principles and advances." *Electromagnetic waves* (Cambridge, Mass.) 147 (2014): 1.
6. Wang, Xueding, Yongjiang Pang, Geng Ku, Xueyi Xie, George Stoica, and Lihong V. Wang. "Noninvasive laser-induced photoacoustic tomography for structural and functional in vivo imaging of the brain." *Nature biotechnology* 21, no. 7 (2003): 803.
7. Xu, Minghua, and Lihong V. Wang. "Photoacoustic imaging in biomedicine." *Review of scientific instruments* 77, no. 4 (2006): 041101.
8. Kruger, Robert A., Cherie M. Kuzmiak, Richard B. Lam, Daniel R. Reinecke, Stephen P. Del Rio, and Doreen Steed. "Dedicated 3D photoacoustic breast imaging." *Medical physics* 40, no. 11 (2013): 113301.
9. Beard, Paul. "Biomedical photoacoustic imaging." *Interface focus* 1, no. 4 (2011): 602-631.
10. Yao, Junjie, Konstantin I. Maslov, Yunfei Shi, Larry A. Taber, and Lihong V. Wang. "In vivo photoacoustic imaging of transverse blood flow by using Doppler broadening of bandwidth." *Optics letters* 35, no. 9 (2010): 1419-1421.

11. Wu, Dan, Lin Huang, Max Jiang, and Huabei Jiang. "Contrast agents for photoacoustic and thermoacoustic imaging: a review." *International journal of molecular sciences* 15, no. 12 (2014): 23616-23639.
12. Doria, Gonçalo, João Conde, Bruno Veigas, Leticia Giestas, Carina Almeida, Maria Assunção, João Rosa, and Pedro V. Baptista. "Noble metal nanoparticles for biosensing applications." *Sensors* 12, no. 2 (2012): 1657-1687.
13. Wang, Yiwen, Xueyi Xie, Xueding Wang, Geng Ku, Kelly L. Gill, D. Patrick O'Neal, George Stoica, and Lihong V. Wang. "Photoacoustic tomography of a nanoshell contrast agent in the in vivo rat brain." *Nano Letters* 4, no. 9 (2004): 1689-1692.
14. Agarwal, A., S. W. Huang, M. O'donnell, K. C. Day, M. Day, N. Kotov, and Shai Ashkenazi. "Targeted gold nanorod contrast agent for prostate cancer detection by photoacoustic imaging." *Journal of applied physics* 102, no. 6 (2007): 064701.
15. Zhang, Q., N. Iwakuma, P. Sharma, B. M. Moudgil, C. Wu, J. McNeill, H. Jiang, and S. R. Grobmyer. "Gold nanoparticles as a contrast agent for in vivo tumor imaging with photoacoustic tomography." *Nanotechnology* 20, no. 39 (2009): 395102.
16. Cheng, Liang, Jingjing Liu, Xing Gu, Hua Gong, Xiaoze Shi, Teng Liu, Chao Wang, Xiaoyong Wang, Gang Liu, Huaiyong Xing, Wenbo Bu, Baoquan Sun, and Zhuang Liu. "PEGylated WS2 nanosheets as a multifunctional theranostic agent for in vivo dual - modal CT/photoacoustic imaging guided photothermal therapy." *Advanced materials* 26, no. 12 (2014): 1886-1893.
17. Ge, Jiechao, Qingyan Jia, Weimin Liu, Liang Guo, Qingyun Liu, Minhuan Lan, Hongyan Zhang, Xiangmin Meng, and Pengfei Wang. "Red - emissive carbon dots for fluorescent, photoacoustic, and thermal theranostics in living mice." *Advanced Materials* 27, no. 28 (2015): 4169-4177.
18. Feng, Qianhua, Yuanyuan Zhang, Wanxia Zhang, Xiaoning Shan, Yujie Yuan, Hongling Zhang, Lin Hou, and Zhenzhong Zhang. "Tumor-targeted and multi-stimuli responsive drug delivery system for near-infrared light induced chemo-phototherapy and photoacoustic tomography." *Acta biomaterialia* 38 (2016): 129-142.
19. Xie, Jin, Seulki Lee, and Xiaoyuan Chen. "Nanoparticle-based theranostic agents." *Advanced drug delivery reviews* 62, no. 11 (2010): 1064-1079.

20. Bharti, Charu, Upendra Nagaich, Ashok Kumar Pal, and Neha Gulati. "Mesoporous silica nanoparticles in target drug delivery system: A review." *International journal of pharmaceutical investigation* 5, no. 3 (2015): 124.
21. Mo, Alexander H., Preston B. Landon, Chris D. Emerson, Chen Zhang, Paula Anzenberg, Siddhartha Akkiraju, and Ratnesh Lal. "Synthesis of nano-bowls with a Janus template." *Nanoscale* 7, no. 2 (2015): 771-775.
22. Mo, Alexander H., Preston B. Landon, Karla Santacruz Gomez, Heemin Kang, Joon Lee, Chen Zhang, Woraphong Janetanakit, Vrinda Sant, Tianyu Lu, David A. Colburn, Siddhartha Akkiraju, Samuel Dossou, Yue Cao, Kuo-Fen Lee, Shyni Varghese, Gennadi Glinskyc and Ratnesh Lal. "Magnetically-responsive silica-gold nanobowls for targeted delivery and SERS-based sensing." *Nanoscale* 8, no. 23 (2016): 11840-11850.
23. Duff, Daniel G., Alfons Baiker, and Peter P. Edwards. "A new hydrosol of gold clusters. 1. Formation and particle size variation." *Langmuir* 9, no. 9 (1993): 2301-2309.
24. Kang, Jinyoung, Dokyoung Kim, Junxin Wang, Yunho Han, Jonathan M. Zuidema, Ali Hariri, Ji-Ho Park, Jesse V. Jokerst, and Michael J. Sailor. "Enhanced performance of a molecular photoacoustic imaging agent by encapsulation in mesoporous silicon nanoparticles." *Advanced Materials* 30, no. 27 (2018): 1800512.
25. Li, Wanwan, and Xiaoyuan Chen. "Gold nanoparticles for photoacoustic imaging." *Nanomedicine* 10, no. 2 (2015): 299-320.
26. Xiang, Liangzhong, Da Xing, Huaimin Gu, Diwu Yang, Lvming Zeng, and Sihua Yang. "Gold nanoshell-based photoacoustic imaging application in biomedicine." In *2006 International Symposium on Biophotonics, Nanophotonics and Metamaterials*, pp. 76-79. IEEE, 2006.
27. Huang, Peng, Jing Lin, Wanwan Li, Pengfei Rong, Zhe Wang, Shouju Wang, Xiaoping Wang, Xiaolian Sun, Maria Aronova, Gang Niu, Richard D. Leapman, Zhihong Nie, and Xiaoyuan Chen. "Biodegradable gold nanovesicles with an ultrastrong plasmonic coupling effect for photoacoustic imaging and photothermal therapy." *Angewandte Chemie International Edition* 52, no. 52 (2013): 13958-13964.
28. El-Brollosy, T. A., T. Abdallah, Mona B. Mohamed, S. Abdallah, K. Easawi, S. Negm, and H. Talaat. "Shape and size dependence of the surface plasmon resonance of gold nanoparticles studied by Photoacoustic technique." *The European Physical Journal Special Topics* 153, no. 1 (2008): 361-364.

29. Yang, Xinmai, Erich W. Stein, S. Ashkenazi, and Lihong V. Wang. "Nanoparticles for photoacoustic imaging." *Wiley interdisciplinary reviews: nanomedicine and nanobiotechnology* 1, no. 4 (2009): 360-368.